Application of Robust Control to a Cryogenic Current Comparator

Marcos Eduardo Bierzychudek, Martin Götz, Ricardo S. Sánchez-Peña, Ricardo Iuzzolino, and Dietmar Drung

***Abstract*— This paper describes the implementation of a digital robust controller in a cryogenic current comparator. The controller was designed applying $\mathcal{H}_\infty$ control theory and it was programmed in a home-made digital unit. Experimental comparisons of the new robust controller with the conventional analog integrator have showed a significant improvement of stability robustness and noise rejection in the system.**

***Index Terms*— Current comparator, $\mathcal{H}_\infty$ control, metrology, resistance measurement, superconducting quantum interference device (SQUID).**

I. Introduction

THE most accurate measurements have been obtained by direct comparison of devices of the same kind, using a sensitive instrument to detect their difference. The uncertainty can be reduced if the user operates on the system until the bridge is balanced, which corresponds to a detector reading equal zero. In terms of control theory, it means that a negative feedback loop is closed. Control theory shows that feedback loops can also be used to reject the effects of unwanted signals, guarantee closed-loop stability, and improve robustness. In addition, the theory provides tools to model systems, design controllers, and evaluates their performances [1]–[3].

This paper presents the application of robust control theory in a cryogenic current comparator (CCC) [4], which is a key module of measurement bridges for resistance comparison at direct current with ultimate accuracy [5]. The CCC is operated in combination with a superconducting quantum interference device (SQUID), a magnetic sensor with unparalleled sensitivity. This sensor measures the noncancelled magnetic flux in the CCC, but it has a nonlinear behavior and limited dynamic range. These features and the high-Q self-resonances of the comparator can lead to instability of the bridge, turning this problem into an excellent test bench for control theory in metrology.

M. E. Bierzychudek is with the Centro de Física y Metrología, Instituto Nacional de Tecnología Industrial, Buenos Aires B1650KNA, Argentina, and also with the Instituto Tecnológico de Buenos Aires, Buenos Aires C1106ACD, Argentina (e-mail: marcosb@inti.gob.ar).

M. Götz and D. Drung are with the Physikalisch-Technische Bundesanstalt, 38116 Braunschweig, Germany.

R. Sánchez-Peña is with CONICET, Buenos Aires C1033AAJ, Argentina, and also with the Instituto Tecnológico de Buenos Aires, Buenos Aires C1106ACD, Argentina (e-mail: rsanchez@itba.edu.ar).

R. Iuzzolino is with the Centro de Física y Metrología, Instituto Nacional de Tecnología Industrial, Buenos Aires B1650KNA, Argentina (e-mail: ricardo.iuzzolino@inti.gob.ar).

The objective of the new digital controller is to improve SQUID performances and stability robustness. For this purpose, the controller has to measure the sensor output and drive a CCC input in order to reach the following specifications:

1) elimination of low frequency magnetic flux in the CCC to fix the current ratio;
2) rejection of interfering signals at SQUID input;
3) rejection of high slew-rate signals at SQUID input;
4) guarantee the closed-loop stability under model uncertainty.

A reduction of the noise floor and disturbing signals at the input of the SQUID can help to decrease the rms value of the rectified wideband components and the degradation of the SQUID's flux-voltage characteristic. This would be particularly useful when operating the CCC bridge in a harsh environment, where the electromagnetic or mechanical distortions are stronger than in high accuracy laboratories.

High slew-rate signals, whose amplitudes exceed the SQUID's intrinsic linear range, can saturate the SQUID or produce an excursion of the SQUID working point from one to another steady state. Note that the magnetic flux at the input of the SQUID during current reversal has larger amplitude than other input signals. The slew rate of the remaining magnetic flux depends on the duration of current reversal, the values of the measured resistors, and on the dynamic differences between the two branches of the bridge. Therefore, a minimum duration time of current reversal that maintains the stability of the bridge exists to a given setup. This fact imposes a lower limit to the period of reversal and to the cancellation of $1/f$ noise. A wideband controller may allow to decrease the duration of current reversal in order to reduce the $1/f$ noise effects.

All these points together will help to minimize the type-A uncertainty and improve the bridge usability.

A. CCC Bridge at a Glance

The CCC setup has been designed and built by Physikalisch-Technische Bundesanstalt (PTB) and Magnicon [6], [7]. Fig. 1 shows a schematic diagram of the CCC-based measurement bridge used to compare two resistors, R_1 and R_2. Each element is connected in series with a current source and a CCC winding. The magnetic flux of the resulting screening current flowing on the surface of the CCC torus is coupled into the pick-up circuit of the SQUID. To set the current ratio (equal to the reverse ratio of the numbers of turns), a feedback is closed through a current source, $i_2(t)$ in this setup.

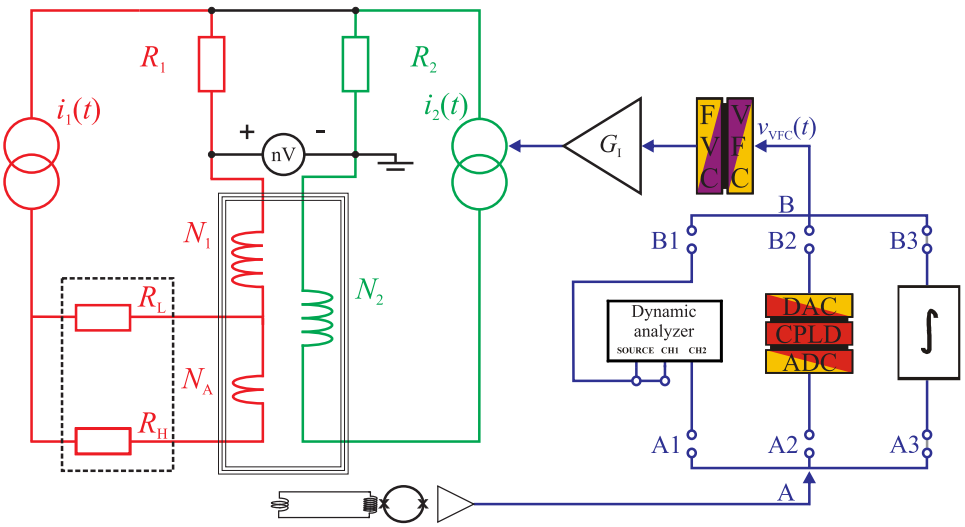

Fig. 1. Simplified scheme of the control loop including the voltage-to-frequency and frequency-to-voltage converters (VFC resp. FVC). For recording the frequency response in open-loop configuration, A and B have to be connected via A1-B1. Connection via A2-B2 corresponds to the closed-loop operation using the digital controller consisting of analog-to-digital and digital-to-analog converters (ADC resp. DAC) with a complex programmable logic device (CPLD) in between. Connection via A3-B3 (shown in gray color) corresponds to the PTB analog integrator.

To full balance the bridge, the voltage difference between both resistors is measured with a nanovoltmeter. A compensation network is used to carry to zero the voltage reading, it consists of an auxiliary winding N_A and a binary compensation unit represented here by R_L and R_H. Proper adjustment of this network can decrease the voltage readings below 100 nV [8].

The controller used in PTB's CCC is an analog integrator implemented in the readout electronics of the SQUID. Its output is available as electromagnetic radiation of variable frequency. The feedback loop can be closed using any current source by means of an optical input and the feedback signal is converted into a voltage using a frequency-to-voltage converter (FVC). After that, the output of the FVC is scaled using a digitally controlled attenuator (G_I) whose attenuation factor can be selected from -27 down to -97 dB. Lastly, the attenuated voltage is added to the main source signal and the resulting voltage is converted into current.

The controller voltage signals or other excitation voltages are converted into electromagnetic radiation with variable frequency using a voltage-to-frequency converter (VFC). The VFC, a fiber optic, and the FVC form an optical link whose transfer function is unitary with a maximum frequency equal to 10 kHz, so this paper is limited to that frequency. The optical link has a central importance in this paper. It will be used to excite the system or to close the feedback loop with different controllers, Fig. 1 shows the possible connections. In fact, the voltage signal at VFC converter, $v_{\mathrm{VFC}}(t)$, is considered as the feedback input.

II. Identification

The identification of the transfer function from the input $V_{\mathrm{VFC}}(s)$ to the output of the SQUID $V_{\mathrm{SQ}}(s)$, $G(s) = V_{\mathrm{SQ}}(s)/V_{\mathrm{VFC}}(s)$, was performed measuring the frequency response with a dynamic analyzer. The instrument was configured in sine sweep mode and connected according to Fig. 1. The analyzer generated a sinusoidal voltage of variable frequency, which was injected into the current source of interest via B–B1 and through the optical link. The instrument measured the excitation voltage and the SQUID output, and calculated the magnitude and phase of their ratio in order to obtain $G(s)$. The output voltage of the SQUID and excitation signal were displayed on an oscilloscope. Therefore, the amplitude of the excitation signal was decreased in case of saturation or an excursion of the SQUID working point from one to another steady state.

Four configurations were selected according to their importance and/or challenge. The most studied setup was 12.9 kΩ against 100 Ω, which is the usual setup to obtain traceability with the integer quantum Hall effect (second *plateau*). In addition, the ratios 1 and 100 MΩ against 12.9 kΩ were studied because the applied currents to the unknown resistors were less than 3 μA, so a high magnetic flux resolution was required. However, the thermal noise of the high value resistors limited the system noise floor. Consequently, a configuration to calibrate a new current amplifier called *ultrastable low-noise current amplifier* (ULCA [9]) was also tested. This device has lower thermal noise, then the SQUID noise dominated the system resolution and therefore this configuration allowed to study the effects of controller performance in the final type-A uncertainty.

The measured transfer functions presented strong dependence on the studied configurations, which was probably produced by leakage currents flowing through the windings. However, the system can measure 100 MΩ with an accuracy lower than 1 $\mu\Omega/\Omega$, hence the current leakage effects have to be negligible at the measurement frequency: 50 mHz approximately. This behavior can be modeled with stray capacitances, but a complete analysis of this problem is beyond the scope of this paper. Based on these observations, a family of models that covers all the possible configurations of the system could be very conservative, hence reducing the performance of the closed-loop system [1], [10]. Thus, an algorithm was developed to identify a family of models in order to design a robust controller for each configuration. The

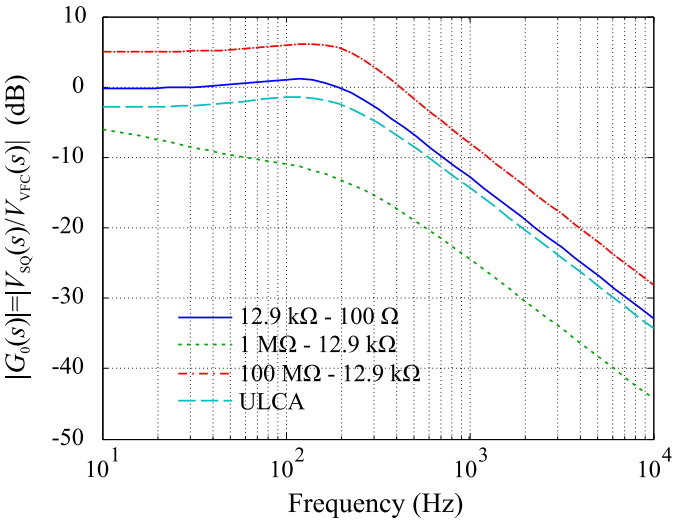

Fig. 2. Nominal model for each working configurations. The feedback for 12.9 kΩ against 100 Ω was closed at source 2 with 5 mA range, 31-turns winding and $G_I = -49.5$ dB. Similar parameters were used for ULCA calibration, but with a 4-turns winding connected to the secondary resistor of 100 Ω and $G_I = -34.5$ dB. For measuring resistors of 1 and 100 MΩ, the feedback was closed in the primary source with a range of 5 μA. With the first resistor, we used the 4029-turns winding and an attenuation of −37 dB, while with the second a 15496-turns winding and $G_I = -29.5$ dB was configured.

nominal model was estimated from experimental data using the subspace algorithm and the prediction error minimization method [11].

The frequency responses of the nominal models, $G_0(s)$, are shown in Fig. 2. They have a dynamic uncertainty close to 5.5% up to 10 kHz, produced mainly by the dynamic analyzer and the system repeatability. After that frequency the knowledge of the system must be considered null, i.e., above 100% uncertain. In this way, the family of models was constructed with the nominal model and a multiplicative dynamic weight that limits the knowledge of the system above 10 kHz.

III. $\mathcal{H}_\infty$ Controller Design and Implementation

The robust controller was designed by an algorithm that optimizes the $\mathcal{H}_\infty$ norm of a certain transfer function, as explained in [1] and [10]. More precisely, the application was posed as a mixed sensitivity problem, which guaranteed stability and disturbance rejection for all closed-loop models in the family of models, which actually included the real physical system. The designed controllers, one for each configuration, behaved like an integrator up to 100 Hz. At that frequency, they reduced the gain slope up to 1 kHz and then they returned to the integrative behavior.

A control unit was designed and implemented to measure the SQUID output, calculate the control equation, and generate the feedback signal in approximately 9 μs and with 100 kHz sampling rate. The acquisition was performed with an 18-bits analog-to-digital converter (ADC) in a unique range of ±0.7 V with a cutoff frequency equal to 15 kHz. The control signal was generated by a 20-bits digital-to-analog converter (DAC) with ±5 V of range and a cutoff frequency of 100 kHz. The control unit had a complex programmable logic device (CPLD) to configure and manage the ADC and DAC converters, and to compute the feedback signal. Because of the number of logic elements (LEs) of the used CPLD, it has 1270 LEs, a limit to the algorithm size was introduced. The control equation was approximated by a difference equation, which was solved sequentially with second-order sections, allowing to represent an equation of order 4 with a 20-bits digital word size. We will show next that the achieved resolution in the calculation produced some numerical errors solving the control equation that limited the controller performance at low frequencies.

The control action depended on the gain from the optical link input to the magnetic flux in the CCC. So, the adjustable attenuator G_I was selected to obtain good sensitivity and wide dynamic range. The first determines the minimum magnetic flux that can be cancelled, hence a bad resolution could generate systematic errors. The dynamic range of the controller limits the amplitude of the distortions that can be cancelled. If the range is larger, the system could reject larger perturbations. Note that these requirements are opposite and a compromise has to be reached. The approach was to set the attenuator gain in order to match the resolution of the DAC with the resolution of the ADC, equal to 0.3 nA for a single turn of the CCC.

IV. Controller Comparison

The performance of the $\mathcal{H}_\infty$ controller ($K_\infty(s)$) and the analog integrator ($K_I(s)$) was compared. First, some measurements of resistors were performed. Then, the controllers were contrasted by means of frequency response measurements of the closed-loop transfer function. This information was complemented with noise spectrum measurements at the SQUID output and temporary step or impulse responses. In addition, a test to study the effects of mechanical distortions was carried out (see [12]).

A. Resistor Measurements

For each configuration some measurements of the resistance ratio were performed, closing the feedback loop consecutively with the integrative and the $\mathcal{H}_\infty$ controller. The results are shown in Fig. 3, where the error bars inform the type-A uncertainty of 48 individual measurements (or 24 in a few cases). Each individual value was taken in a 20 s cycle, which included a current reversal.

Only the resistors of 100 Ω and 12.9 kΩ were in a stabilized air bath within the range of 22.90 °C–22.94 °C. So, the type-A uncertainties of the measurements involving high value resistors were affected by the laboratory temperature instability, ±0.2 °C. The nominal linear temperature coefficients of the 1 and 100 MΩ resistors were 0.06 and 5 $\mu\Omega/\Omega$, respectively.

In the measurement of 100 MΩ versus 12.9 kΩ, the $\mathcal{H}_\infty$ controller was designed and used with two values of the adjustable attenuator, $G_I = -47$ dB and $G_I = -42$ dB. The first configuration had a better control resolution, but the SQUID working point moved from one to another steady state with a duration of current reversal equal to 0.2 s due to the limited dynamic range of the controller, hence a duration

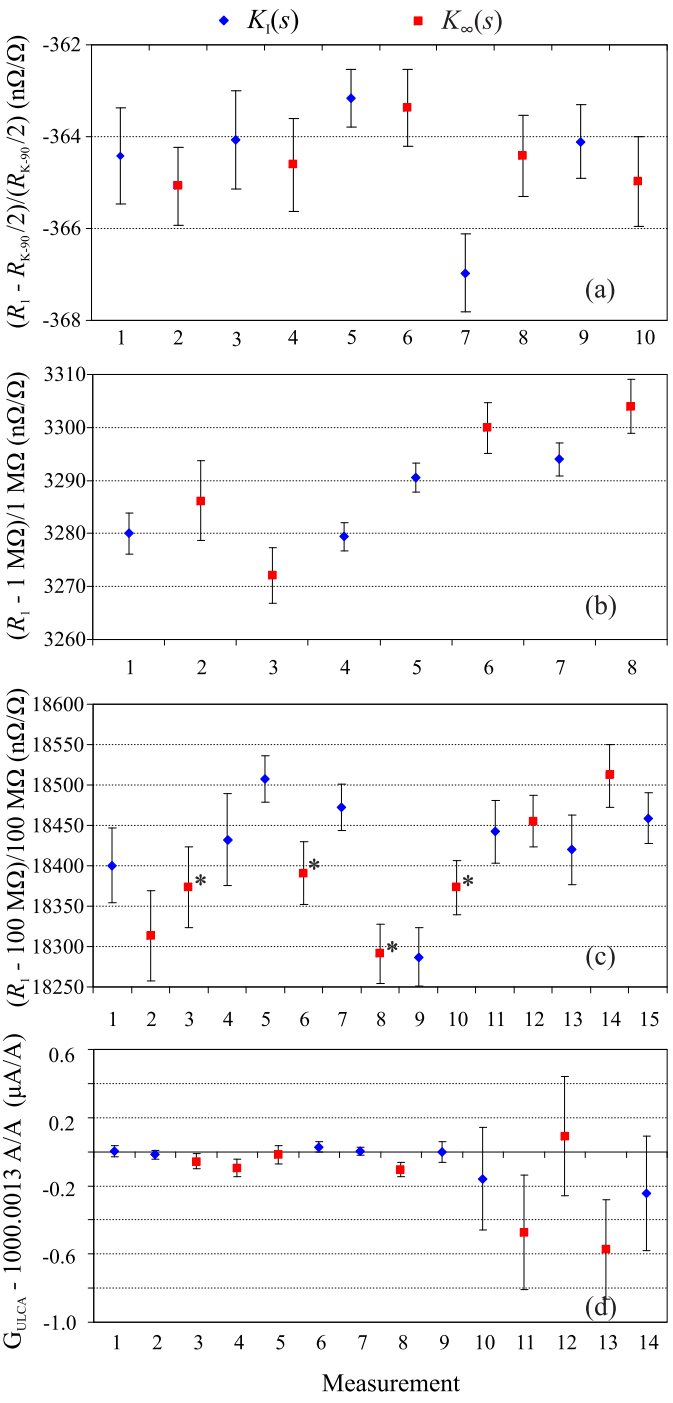

Fig. 3. Measurements of R_1 to the ratio (a) 12.9 kΩ versus 100 Ω, (b) 1 MΩ versus 12.9 kΩ, and (c) 100 MΩ versus 12.9 kΩ. (d) Measured value of ULCA's amplification. The results obtained with the integrative controller are shown with blue diamonds, while red squares represent the corresponding values taken with the $\mathcal{H}_\infty$ controller. In (c), the $\mathcal{H}_\infty$ controller was designed and used with two values of the adjustable attenuator, $G_I = -47$ dB and $G_I = -42$ dB, the second configuration is indicated with asterisks.

of 0.3 s was configured. The faster duration of current reversal could be successfully stabilized using the second configuration because the controller had a larger dynamic range. Fig. 3(c) shows the results for both configurations; the latter is indicated by asterisks. In the case of the ULCA calibration (Fig. 3(d)) the current in the amplifier input was 13 nA and the last five measurements were taken with a current ten times smaller.

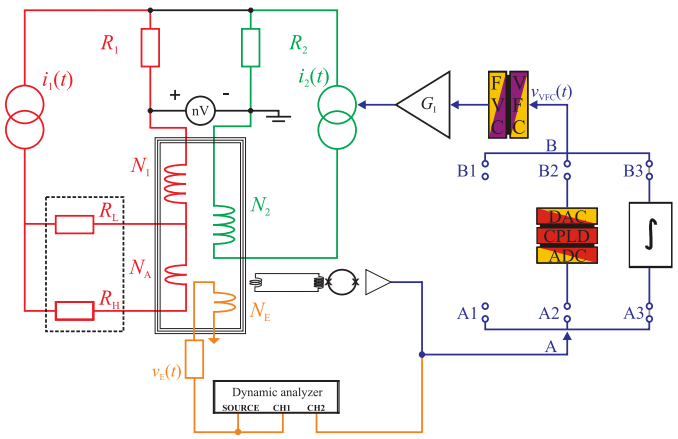

Fig. 4. Experimental setup used to measure the transfer function of the open- and closed-loop system from an excitation winding.

A good compatibility was found, therefore, the new controller can be used in routine measurements of resistors. However, larger standard deviations were obtained with the digital controller for 1 MΩ and ULCA configurations, e.g., in Fig. 3(d) the type-A uncertainty obtained with $K_I(s)$ is two times lower. This was produced by numerical errors in the calculation of the control equation that generated low frequency noise.

B. Closed-Loop Frequency Response

The frequency response of the closed- and open-loop system was measured with a dynamic analyzer (see Fig. 4). It excited the CCC with a voltage $V_E(s)$, which was magnetically coupled to the CCC using N_E with a resistor connected in series. The instrument measured the applied voltage and the output of the SQUID, and reported the ratio between both.

The rejection of the input signals $V_E(s)$, including exogenous distortion, in the SQUID output can be quantified as $|V_{SQ}(s)/V_E(s)|$ with $s = \jmath\omega$ fixed at the frequency of interest, e.g., the power line frequency or its harmonics. So, the closed-loop transfer function obtained with both controllers can be compared, the one with lower amplification has better distortion rejection.

Fig. 5 shows the frequency responses for the ratio 12.9 kΩ versus 100 Ω with the digital and analog controller. $K_I(s)$ was configured with several values of the input feedback attenuator, from −59.5 up to −42 dB. When this gain was increased, the peak of the magnitude also increased until the closed-loop system lose its stability (with $G_I = -39.5$ dB). This showed clearly that the bandwidth of the integrative controller was limited by the CCC's resonant frequency [13]. However, the controller designed by $\mathcal{H}_\infty$ control presented a larger bandwidth and a better rejection of distortion. It reduced the magnitude of the transfer function by 20 dB up to 500 Hz and at that frequency the difference was 40 dB compared with the usual configuration at PTB ($K_I(s)$ with $G_I = -49.5$ dB).

The configuration 1 MΩ versus 12.9 kΩ presented strong differences in the frequency response depending on which current source was controlled. Fig. 6 shows several measurements with the integrative control connected to both

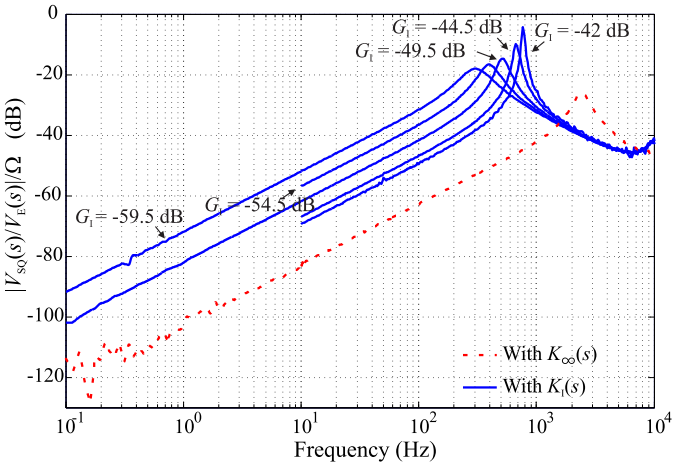

Fig. 5. Frequency response measurements of the closed-loop system ready to measure 12.9 kΩ versus 100 Ω with the integrative and the digital controller. The measurement was repeated with $K_I(s)$ and several values of G_I.

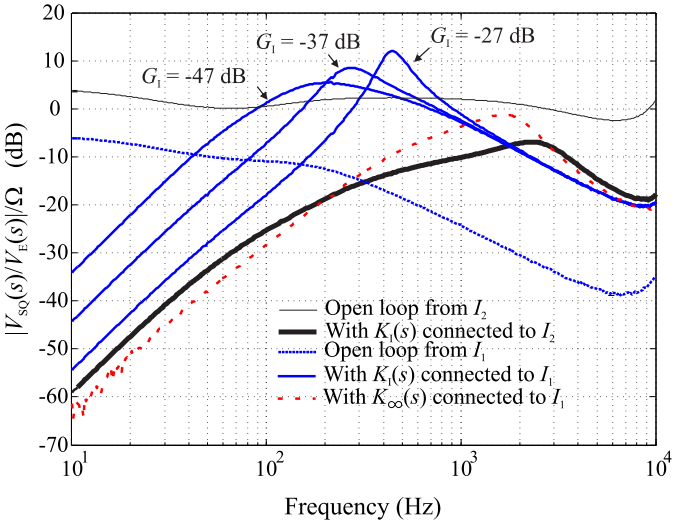

Fig. 6. Frequency response measurements performed with the configuration 1 MΩ versus 12.9 kΩ.

sources and with $K_\infty(s)$ connected to the primary source. The open-loop transfer functions from I_1 and I_2 were also included. When the integrative feedback is injected in $I_2(s)$, the measured closed-loop frequency response is faster compared with other configurations, because the open-loop response from that input (thin black line) is almost flat. Instead, the feedback current is attenuated at high frequencies when it is injected into $I_1(s)$ (blue dotted line). $K_\infty(s)$ was implemented in this source due to the limited resources in the CPLD and the measured closed-loop frequency response was 10 dB lower than the faster response obtained with the integrative controller connected to the same current source.

Fig. 7 shows the measurements of the 100 MΩ versus 12.9 kΩ ratio. When the feedback was closed with $K_I(s)$ and $G_I = -47$ dB the frequency response (blue line) was equal to the one obtained at open loop from the same excitation winding (thin black line). This was produced because the

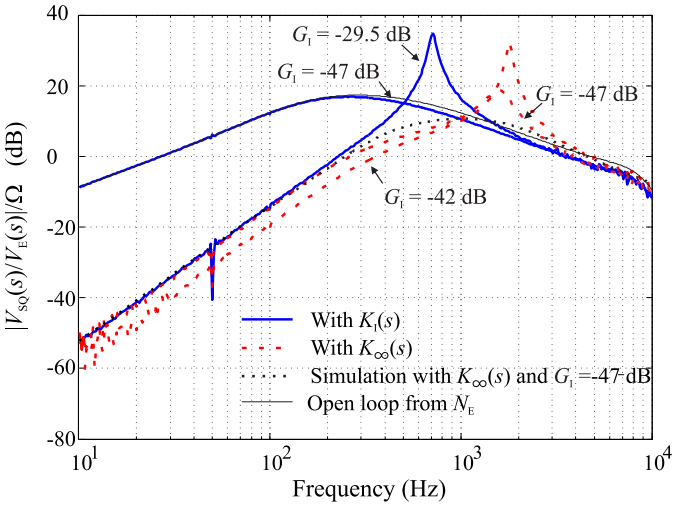

Fig. 7. Frequency response measurements performed with the configuration 100 MΩ versus 12.9 kΩ. A simulation of the closed-loop frequency response is included.

TABLE I

PEAK VALUE AND FREQUENCY OF $|S(j\omega)|_\infty$ FOR EACH CONFIGURATION AND CONTROLLER. IN THE 1 MΩ VERSUS 12.9 kΩ SETUP, THE PRESENTED RESULTS WERE OBTAINED USING THE DATA WHICH INVOLVE THE PRIMARY CURRENT SOURCE

Ratio	Controller	$\lvert S(j\omega)\rvert_\infty$	$\frac{\omega}{2\pi}$
12.9 kΩ vs 100 Ω	$K_I(s)$ with $G_I = -49.5$ dB	4.9 V/V	3.4 kHz
	$K_I(s)$ with $G_I = -42$ dB	23.0 V/V	4.8 kHz
	$K_\infty(s)$	5.3 V/V	15.3 kHz
1 MΩ vs 12.9 kΩ	$K_I(s)$ with $G_I = -27$ dB	3.5 V/V	2.8 kHz
	$K_\infty(s)$	2.4 V/V	12.0 kHz
100 MΩ vs 12.9 kΩ	$K_I(s)$ with $G_I = -29.5$ dB	10.7 V/V	4.5 kHz
	$K_\infty(s)$ with $G_I = -47$ dB	3.4 V/V	10.0 kHz

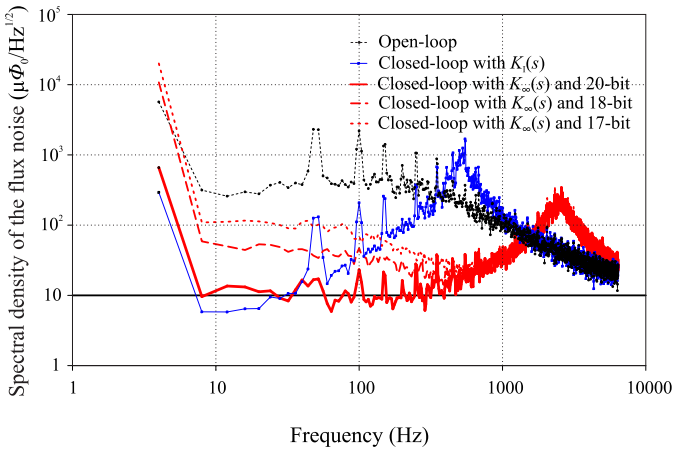

Fig. 8. Spectral density of the magnetic flux noise in the SQUID superconducting ring depending on the frequency. The system was configured to measure 12.9 kΩ versus 100 Ω. Three measurements are shown with $K_\infty(s)$; in the first case all the resources of the CPLD were used and in the other measurements the size of the calculation word was intentionally reduced by 2 and 3 bits. The used word sizes are presented.

controller's gain was not strong enough. In fact, the standard configuration for this ratio used $G_I = -29.5$ dB. In this case, $K_\infty(s)$ with $G_I = -42$ dB reduced the magnitude of the

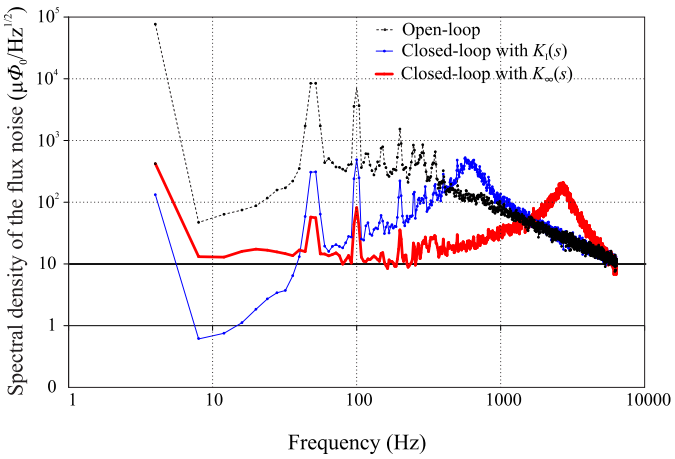

Fig. 9. Spectral density of the magnetic flux noise in the SQUID superconducting ring depending on the frequency. The CCC was ready to the calibration of the ULCA amplifier.

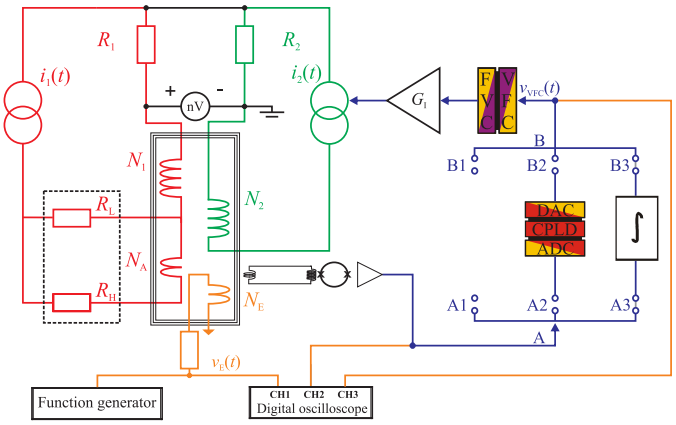

Fig. 10. Experimental setup used to measure the step and impulse responses of the closed-loop CCC. A function generator excited the system. A digital oscilloscope measured the input signal, the output of the SQUID and the input voltage to the optical link [$v_{\mathrm{VFC}}(t)$].

frequency response by 10 dB at frequencies lower than 400 Hz and by 20 dB at 700 Hz.

The measured transfer function was affected by the dynamics of the excitation winding N_E. An independent result is the peak value of the transfer function $S(s) = 1/(1 + G(s)K(s))$ with $s = \jmath\omega$ and $G(s) = V_{\mathrm{SQ}}(s)/V_{\mathrm{VFC}}(s)$. First, the transfer functions from N_E at closed loop and open loop were identified, and then the infinity norm of the first model divided by the second was calculated. Table I shows the peak value for each controller and configuration. The new controller improved the closed-loop performance in all the cases.

C. Spectral Density of Flux Noise

In this section, some spectral densities of flux noise in SQUID input are presented. This is the usual figure of merit for SQUID-based system [14], [15]. However, the measured noise can be affected by external perturbations and a complete isolation of the CCC bridge is, at least, a challenging task. So, we performed this experiment as a comparative study of controller's performance.

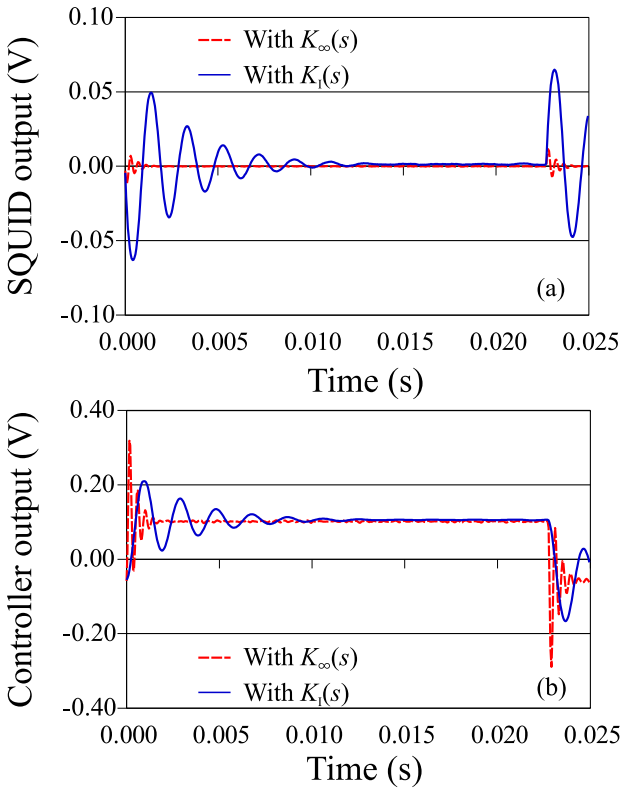

Fig. 11. Response of the closed-loop CCC to square wave excitations using the digital and the analog controller. (a) and (b) Outputs of the SQUID and the controller are presented, respectively.

The results for the ratio 12.9 kΩ versus 100 Ω are shown in Fig. 8. In addition, the results for the calibration of the ULCA amplifier are presented in Fig. 9. In both cases, the closed-loop system with the controller designed by $\mathcal{H}_\infty$ presented a lower noise floor from 30 up to 1 kHz. In this way, the rms noise at the SQUID input was reduced by 35% or 25%. However, the noise floor obtained with $K_\infty(s)$ was worse at low frequencies because the numerical errors in the control unit produced a noise limit equal to 10 $\mu\Phi_0/\sqrt{\mathrm{Hz}}$. This phenomenon was clearly observed in the ULCA setup because the amplifier had a lower noise level than the thermal noise of a 12.9 kΩ resistor at room temperature. To test this problem, the measurement was repeated with the $\mathcal{H}_\infty$ controller reducing by 2 or 3 bits the word size used to calculate the control equation. The low frequency noise got worse with each case (see Fig. 8).

D. Step and Impulse Responses

The step and impulse responses can be used to compare the controllers. We focused in two parameters, the overshoot, and the time constant. The first one gives an idea of the maximum output for a given input, so it can be related to the closed-loop system stability. The time constant is related to the controller bandwidth; a lower time constant is equivalent to a faster controller.

The experimental setup is depicted in Fig. 10; the excitation signal was injected through N_E. The SQUID output, the excitation voltage, and the feedback signal were measured with

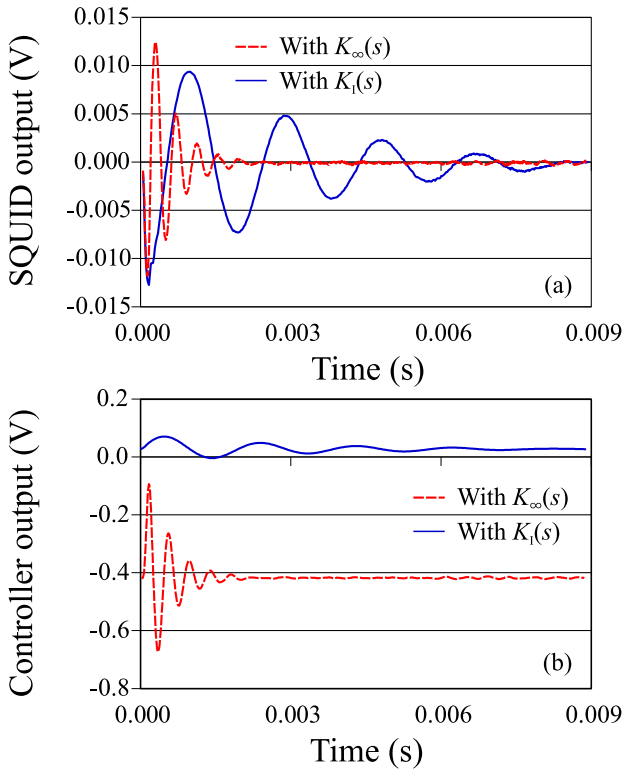

Fig. 12. Response of the closed-loop CCC to impulse excitations using the digital and the analog controller. (a) and (b) Outputs of the SQUID and the controller are presented, respectively.

a digital oscilloscope. The CCC was configured to measure the ratio 12.9 kΩ versus 100 Ω and the feedback was closed alternately with each controller.

Figs. 11 and 12 depict the step and impulse responses. The new controller reduced the time constant in both cases. In addition, the overshoot in the SQUID output was strongly reduced with the step excitation. However, this parameter could not be improved with the impulse excitation.

The maximum amplitude of the excitation signal without losing closed-loop system stability can also be studied. The peak value of the excitation was increased until excursions of the SQUID working point were observed. $K_\infty(s)$ could manage a square wave with an amplitude up to 2.75 times the maximum value that the integrator could drive. In the case of the pulse train, the same behavior was found but with a margin equal to 50%.

V. Conclusion

The $\mathcal{H}_\infty$ control theory was successfully applied to four configurations of the PTB's CCC. The designed controllers were implemented with a home-made digital unit and this new setup increased stability robustness, distortion rejection, and reduced the effective noise in the SQUID input. These improvements were possible due to the larger bandwidth of the $\mathcal{H}_\infty$ controller in comparison with the integrative (analog) controller.

The standard deviations of the resistance measurements with the new controllers were equal or worse than the obtained values with the integrative controller. This fact demonstrated a deficient cancellation of the magnetic flux at the measurement frequency due to the numerical errors in the calculation of the control equation. The type-A uncertainty can be improved increasing the binary word size in the calculation. To accomplish this, the CPLD has to be replaced by a state-of-the-art programmable logic device. In addition, this may help to reduce the delay between measurement and action, increasing the controller bandwidth.

References

[1] R. Sánchez-Peña and M. Sznaier, *Robust Systems: Theory and Applications*, 1st ed. Hoboken, NJ, USA: Wiley, 1998.

[2] G. C. Goodwin, S. F. Graebe, and M. E. Salgado, *Control System Design*, 1st ed. Englewood Cliffs, NJ, USA: Prentice-Hall, 2000.

[3] M. Schulz, *Control Theory in Physics and Other Fields of Science* (Springer Tracts in Modern Physics), 1st ed. Berlin, Germany: Springer, 2006.

[4] M. E. Bierzychudek, R. Sánchez-Peña, A. Tonina, R. Iuzzolino, D. Drung, and M. Götz, "Application of robust control to a cryogenic current comparator," in *CPEM Dig.*, Ottawa, ON, Canada, Jul. 2016, pp. 1–2.

[5] J. M. Williams, "Cryogenic current comparators and their application to electrical metrology," *IET Sci. Meas. Technol.*, vol. 5, no. 6, pp. 211–224, Nov. 2011.

[6] M. Götz *et al.*, "Improved cryogenic current comparator setup with digital current sources," *IEEE Trans. Instrum. Meas.*, vol. 58, no. 4, pp. 1176–1182, Apr. 2009.

[7] M. Götz, E. Pesel, and D. Drung, "A compact 14-bit cryogenic current comparator," in *CPEM Dig.*, Rio de Janeiro, Brazil, Aug. 2014, pp. 684–685.

[8] D. Drung, M. Götz, E. Pesel, H. J. Barthelmess, and C. Hinnrichs, "Aspects of application and calibration of a binary compensation unit for cryogenic current comparator setups," *IEEE Trans. Instrum. Meas.*, vol. 62, no. 10, pp. 2820–2827, Oct. 2013.

[9] D. Drung, M. Götz, E. Pesel, and H. Scherer, "Improving the traceable measurement and generation of small direct currents," *IEEE Trans. Instrum. Meas.*, vol. 64, no. 11, pp. 3021–3030, Nov. 2015.

[10] M. E. Bierzychudek, R. S. Sánchez-Peña, and A. Tonina, "Identification and control of a cryogenic current comparator using robust control theory," *IEEE Trans. Instrum. Meas.*, vol. 64, no. 12, pp. 3451–3457, Dec. 2015.

[11] L. Ljung, *System Identification Toolbox—User's Guide, Revised for Version 9.0* , MATLAB-The Math Works, Mar. 2014.

[12] M. E. Bierzychudek, M. Götz, and M. Schmelzer, "Operation of a cryogenic current comparator in presence of mechanical vibrations," in *CPEM Dig.*, Ottawa, ON, Canada, Jul. 2016, pp. 1–2.

[13] J. Kinoshita *et al.*, "Self-balancing resistance ratio bridge using a cryogenic current comparator," *IEEE Trans. Instrum. Meas.*, vol. 38, no. 2, pp. 290–292, Apr. 1989.

[14] J. Clarke and A. I. Braginski, *The SQUID Handbook: Fundamentals and Technology of SQUIDs and SQUID Systems*, vol. 1. Hoboken, NJ, USA: Wiley, 2004.

[15] P. Gutmann, "A comparison of the cryogenic current comparator and the Josephson potentiometer in resistance bridges using their figures of merit," *IEEE Trans. Instrum. Meas.*, vol. 42, no. 2, pp. 385–390, Apr. 1993.

Marcos Eduardo Bierzychudek received the Electronics Engineering Degree from the Universidad de Buenos Aires, Buenos Aires, Argentina, in 2006, and the Ph.D. degree in engineering from the Instituto Tecnológico de Buenos Aires, Buenos Aires, in 2016.

In 2005, he joined the Quantum Electrical Metrology Laboratory, Instituto Nacional de Tecnología Industrial, Buenos Aires. His current research interests include the applications of control theory and low-noise electronics in electrical metrology.

Martin Götz was born in Erfurt, Germany, in 1968. He received the Diploma and Ph.D. degrees in physics from Friedrich Schiller University, Jena, Germany, in 1992 and 1997, respectively.

He has been with Physikalisch-Technische Bundesanstalt, Braunschweig, Germany, since 1999. His current research interests include the further improvement of cryogenic current comparator-based setups and applications of the quantum Hall effect in electrical metrology.

Ricardo S. Sánchez-Peña (S'86–M'88–SM'00) received the Electronics Engineering Degree from the University of Buenos Aires (UBA), Buenos Aires, Argentina, in 1978, and the M.Sc. and Ph.D. degrees in electrical engineering from the California Institute of Technology, Pasadena, CA, USA, in 1986 and 1988, respectively.

From 1977 to 2004, he was with CITEFA, CNEA, and with the space agencies CNIE and CONAE. He collaborated with NASA, the German (DLR), and Brazilian (CTA/INPE) space agencies. He was a Full Professor at UBA from 1989 to 2004, a Senior Researcher at the Institució Catalana de Recerca i Estudis Avançats, Universitat Politècnica de Catalunya, Barcelona, Spain, from 2005 to 2009, and a Visiting Professor/Researcher at several universities in the U.S. and EU. He was a Consultant of ZonaTech, Scottsdale, AZ, USA, Alstom-Ecotecnia, Spain, and STI and VENG, Argentina. Since 2009, he has been the Director of the Ph.D. Department with the Buenos Aires Institute of Technology, Buenos Aires, and a Principal Investigator with the Consejo Nacional de Investigaciones Científicas y Técnicas, Argentina. He was involved in identification and control techniques to practical problems in engineering and medicine. He has authored three books and more than 140 journal and conference papers.

Dr. Sánchez-Peña received the *Premio Consagración* in Engineering by the National Academy of Exact, Physical and Natural Sciences, Argentina, the *Group Achievement* Award from NASA, and the *Ingeniero Eminente* award from the IEEE.

Ricardo Iuzzolino was born in Argentina in 1970. He received the Diploma degree in electronic engineering from the Universidad de Buenos Aires, Buenos Aires, Argentina, in 2003, and the Ph.D. degree from Technische Universität Braunschweig, Braunschweig, Germany, in 2011, with a focus on Josephson waveforms characterization of sigma-delta ADC for data acquisition in metrology.

In 1997, he joined the Electricity Division, Instituto Nacional de Tecnología Industrial Buenos Aires. He is involved in quantum electrical standards (Josephson voltage standard), dc voltage measurements, dc-ac resistance measurement, sampling techniques, and digital signal processing. His current research interests include physics, electronics, DSP, sampling techniques, modeling and numerical simulation, and computer science.

Dietmar Drung was born in Mühlacker, Germany, in 1958. He received the Dipl.-Ing. and Dr.-Ing. degrees in electrical engineering from the University of Karlsruhe, Karlsruhe, Germany, in 1982 and 1988, respectively.

He was a Researcher with the University of Karlsruhe from 1983 to 1988. In 1988, he joined Physikalisch-Technische Bundesanstalt, Berlin, Germany, where he was involved in superconducting quantum interference devices (SQUIDs) and SQUID readout electronics. In 2009, he became a Senior Scientist in superconducting sensors. His current research interests include the development of low-noise amplifiers and measurement systems for magnetic sensing and electrical metrology.